Nanoscale

REVIEW

View Article Online
View Journal | View Issue

Cite this: *Nanoscale*, 2025, **17**, 23896

Donor–acceptor conjugated polymers as high-mobility semiconductors: prospects for organic thermoelectrics

Prithwish Biswas, Lingcheng Kong and Zhiting Tian *

Donor–acceptor conjugated polymers are emerging as a new class of organic semiconductors, where the donor and acceptor moieties function as hole and electron transporters, respectively. The potential of being doped as both p-type and n-type makes them attractive for scalable manufacturing, and they have been widely explored for organic photovoltaics. They can be particularly appealing for organic thermoelectrics, primarily due to their high interchain mobility alongside intrachain mobility. The high intrinsic mobility, resulting from the push–pull effect of the donor–acceptor moieties, ensures high electrical conductivity with minimal doping, which is crucial for maintaining a high Seebeck coefficient in thermoelectric materials. In this review, we explain the molecular structure and energetics, as well as their relationship to the electronic structure of donor–acceptor polymers. We also review the existing literature on how structural and energetic modifications can be implemented to modulate interchain transport, intrachain transport, and doping efficiencies. Based on these, we propose that improvements in molecular design, characterization methods, and the integration of data science and machine learning can accelerate research on donor–acceptor polymers for thermoelectrics and beyond.

Received 20th May 2025,
Accepted 30th September 2025

DOI: 10.1039/d5nr02141c

rsc.li/nanoscale

1. Introduction

According to the US Department of Energy, 67% of energy is discarded as waste heat,[1] which increases operational costs and carbon footprint. Hence, harvesting of waste heat is essential as a major step towards solving the energy crisis, which

Sibley School of Mechanical and Aerospace Engineering, Cornell University, Ithaca, NY 14853, USA. E-mail: zhiting@cornell.edu

Prithwish Biswas

Prithwish Biswas is a Postdoctoral Associate in the Sibley School of Mechanical and Aerospace Engineering at Cornell University. His research focuses on the electronic and optical properties of materials for thermoelectric energy harvesting and electromagnetic interference shielding. He earned his Ph.D. in Chemical Engineering from UC Riverside in 2023, where he studied far-from-equilibrium kinetics and transport in reactive materials for thermochemical energy conversion. He has authored over 30 research articles with an h-index of 15 and received the competitive UC Dissertation Fellowship and the NSF Future Faculty Workshop Award.

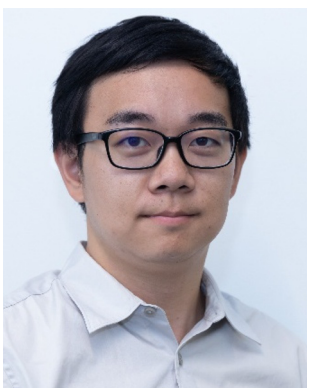

Lingcheng Kong

Lingcheng Kong is a doctoral student in the Department of Mechanical and Aerospace Engineering at Cornell University. He received his M.S. in Mechanical Engineering from Cornell University in 2022 and his B.S. in Mechanical Engineering from the University of Wisconsin–Madison in 2020. His research interests lie in the areas of polymer materials and thermal science, with a focus on thermal transport and energy applications.

has been traditionally done by inorganic thermoelectric devices.[2] The performance of thermoelectric materials is measured by the thermoelectric figure of merit $zT = \frac{\sigma S^2}{k} T$, where σ is the electrical conductivity, S is the Seebeck coefficient, k is the thermal conductivity, and T is the temperature. Crystalline inorganic semiconductors such as metal chalcogenides and metal oxides offer a high zT value of 2.[3] However, there have been emerging efforts in employing organic semiconductors, particularly conjugated polymers,[4,5] which have the adaptability to be manufactured by scalable ink-based printing processes while ensuring the flexibility of the manufactured devices.[6] Although some of the highest power factors have been achieved for p-type organic materials, such as p-doped PEDOT poly(3,4-ethylenedioxythiophene) has demonstrated a power factor of over ~500 μW m^{-1} K^{-2},[7] there is still a dearth of high performing n-type materials as n-type doping is inherently unstable in ambient air because the shallow highest occupied molecular orbital (HOMO) level of the dopants at the neutral state results in their oxidation.[8,9]

Donor–acceptor polymers are copolymers of hole-transporting (donor) and electron-transporting (acceptor) monomers (Fig. 1(a)). Since the donor unit can be doped as p-type or the acceptor unit as n-type, donor–acceptor polymers facilitate ambipolar charge transport.[10–12] The electron-rich donors push electrons, and the acceptors with high electron affinity pull electrons through the backbone, resulting in the successive push–pull effect at finite temperatures.[13,14] Because of this push–pull effect, the donor moieties have a partial positive charge, whereas the acceptor moieties have a partial negative charge when copolymerized. Additionally, by proper selection of the donor and acceptor combinations based on the energy offset between the HOMO level of the isolated donor molecule and the lowest unoccupied molecular orbital (LUMO) level of the isolated acceptor molecule, the bandgap of the resulting donor–acceptor can be precisely tuned leading to either semiconducting or metallic properties.[8,15] When the HOMO of the donor is higher than the LUMO of the acceptor, the copolymer is metallic, whereas when the HOMO of the donor is lower than the LUMO of the acceptor, the copolymer is semiconducting.[16] The LUMO of the acceptor contributes to the conduction bands, and the HOMO of the donor contributes to the valence bands of the copolymer (Fig. 1(b)), resulting in a narrower gap in comparison to that of conventional hole-transporting donor–donor or electron-transporting acceptor–acceptor conjugated polymers. For thermoelectrics, a narrow bandgap between 6–10 k_BT (~0.1–0.3 eV at T = 298 K) yields optimal performance. This is because a narrow bandgap results in higher σ ensuring considerable population of conduction bands at moderate temperatures. Simultaneously, the Fermi level can be placed a few k_BT inside the conduction/valence band *via* minimal doping, maintaining a large asymmetry in carrier population, yielding a high S.[17] Thus, the donor–acceptor polymers where bandgap can be tuned (0–1 eV) and reduced by proper selection of donor and acceptor moieties are attractive. In conventional conjugated polymers, interchain transport relies on π–π stacking, a short-range and weak van der Waals (vdW) interaction between the aromatic rings. While π–π stacking enables molecular orbital-overlap responsible for band formation, such weak, local interactions are insufficient to enforce complete alignment of all the aromatic rings on adjacent chains.[18] In donor–acceptor polymers, long-range dipolar interactions can facilitate alignment of the aromatic rings on the adjacent chains and increase the probability of π–π stacking, promoting band formation by extending interchain conjugation.[19,20] Additionally, the parallel stacking of donor and acceptor moieties on different chains results in an interchain push–pull effect facilitating extended band formation (Fig. 1(a)). All of these effects collectively result in high carrier mobilities of >1 cm^2 V^{-1} s^{-1} in donor–acceptor polymers, which is higher than most organic semiconductors.[21] Increasing carrier concentration by doping negatively impacts the S. Thus, the high mobility of the donor–acceptor polymers can be leveraged to achieve a high σ with minimal extent of doping without sacrificing the S.[22] The ability to be used as both p-type and n-type materials also makes the large-scale fabrication of thermoelectric devices with donor–acceptor polymers easier.

Although extensive studies have been performed on donor–acceptor polymers from the perspective of photovoltaic and organic transistors, donor–acceptor polymers are relatively new to the field of thermoelectrics. Fundamentally, they are a combination of semiconductors that can be potentially doped both p-type and n-type.[23,24] This not only eases manufacturing and processability but also provides more options for high-mobility n-type organic semiconductors, which are relatively rare.

To summarize, donor–acceptor polymers have the following advantages over conventional conjugated polymers: (i) a broader molecular design space that enables precise bandgap tuning through various donor and acceptor combinations, (ii) partial charges on donor and acceptor leads to small dipole moments along backbone strengthening interchain coupling

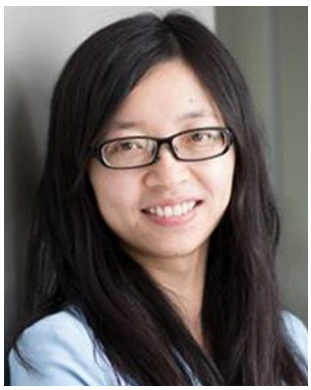

Zhiting Tian

Zhiting Tian is the Eugene A. Leinroth Sesquicentennial Faculty Fellow Professor at the Sibley School of Mechanical and Aerospace Engineering at Cornell University. Zhiting earned her Ph.D. from MIT in 2014. Her research focuses on micro/nanoscale heat transfer, thermal energy systems, and thermal transport in quantum and biological materials. She has published over 90 research articles and has an h-index of 39. Zhiting is an ASME Fellow and a recipient of the highly prestigious Presidential Early Career Award for Scientists and Engineers (PECASE) award besides early career awards from NSF, ONR, AFOSR, and DARPA.

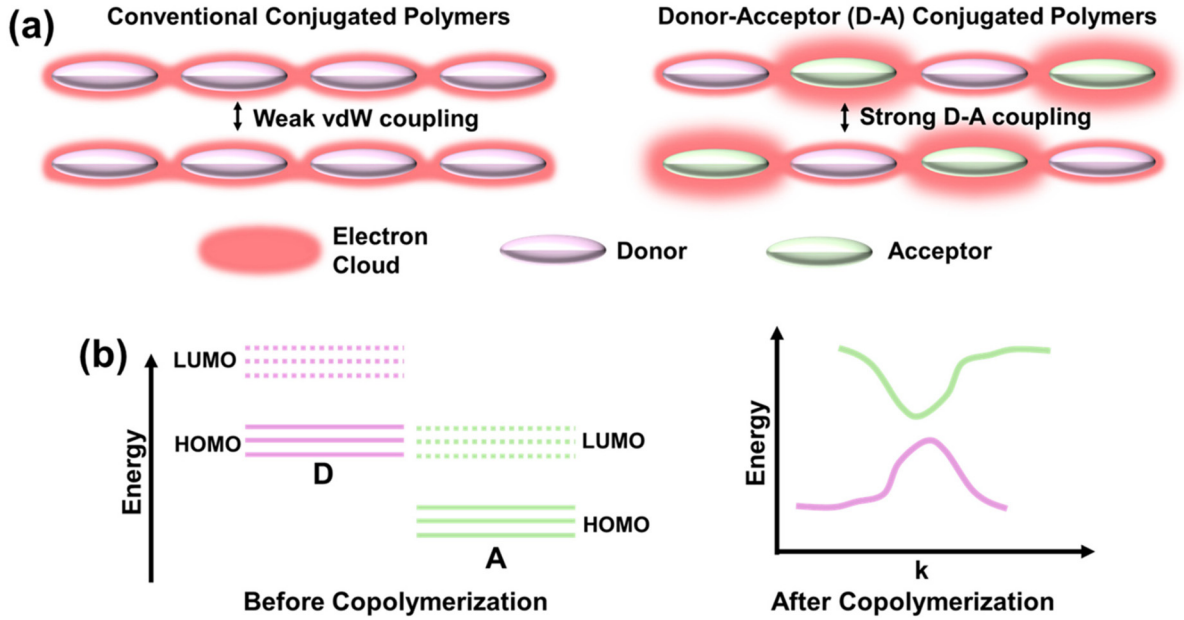

Fig. 1 (a) The electron affinity difference between the donor and acceptor leads to the push–pull effect, which creates intrachain dipoles, which in turn result in stronger interchain coupling relative to the conventional conjugated polymers which have weak interchain vdW coupling. (b) Before copolymerization, the HOMO level of the donor is higher than the LUMO level of the acceptor, and after copolymerization, the donor forms the valence band, whereas the acceptor states form the conduction band, making the donor–acceptor copolymer a semiconductor.

beyond simple vdW stacking, (iii) the ability to being doped as both p and n type eases manufacturing. The objective of this review is to provide an understanding of how donor–acceptor combinations, molecular structures of donors and acceptors, and different processing methods affect the thermoelectric and charge transport properties of donor–acceptor polymers. The review also highlights the perspective for further development of donor–acceptor polymer thermoelectrics, including the necessity for in-plane k measurements of these polymers, alternative methods for precise measurement of carrier concentration and mobility, and the introduction of artificial intelligence and machine learning (ML) to predict thermoelectric properties based on structure–property relationship data. Better understanding and characterization of structure-charge transport relationships will encourage the use of organic thermoelectrics in the long run, taking a step towards bridging the gap between inorganic and organic thermoelectrics.

2. Molecular structure of donor and acceptor moieties

In donor–acceptor polymers, the copolymers used as building blocks for donor and acceptor moieties are basically polymers that can be doped p-type or n-type in an isolated form. Hence, the donor moieties are commonly made up of thiophene derivatives, whose molecular structure is analogous to that of other p-type polymers such as PEDOT and P3HT. The acceptor part is generally made of a diimide derivative such as perylene diimide (PDI) or a derivative of diketo pyrrolopyrrole (DPP). Fig. 2(a) shows examples of donor–acceptor polymers,[25–27] Fig. 2(b) shows some examples of commonly used acceptor moieties, and Fig. 2(c) shows the donor moieties. Therefore, donor–acceptor polymers possess the ability to be doped as both n-type and p-type, as either the acceptor part can be doped by an n-type dopant or the donor part can be doped by a p-type dopant.

3. Energetics associated with charge transport in donor–acceptor polymers

To understand the band structure of the donor–acceptor polymer, one has to begin with the electronic structure of the isolated donor and the acceptor molecules, which are the building blocks of these polymers. Fig. 3(a) shows the HOMO and LUMO levels of different donor and acceptor moieties. As mentioned above, the copolymerization of donor and acceptor systems results in either metallic or semiconducting electronic structures. The extent of charge transfer is directly related to the energy difference between the HOMO level of the donor and the LUMO level of the acceptor.[28] Donor–acceptor combinations of Naphthalene-TCNQ, DMeO-BTBT-2,5 F_2TCNQ, and DPTTA-F_4TCNQ have been investigated.[28] The HOMO of the donor is lower than the LUMO of the acceptor in Naphthalene-TCNQ and DMeO-BTBT-2,5 F_2TCNQ, making these systems narrow bandgap semiconductors. The HOMO of the donor is much higher than the LUMO of the acceptor in DPTTA-F_4TCNQ, resulting in the complete delocalization of electrons along the polymer backbone leading to a metallic

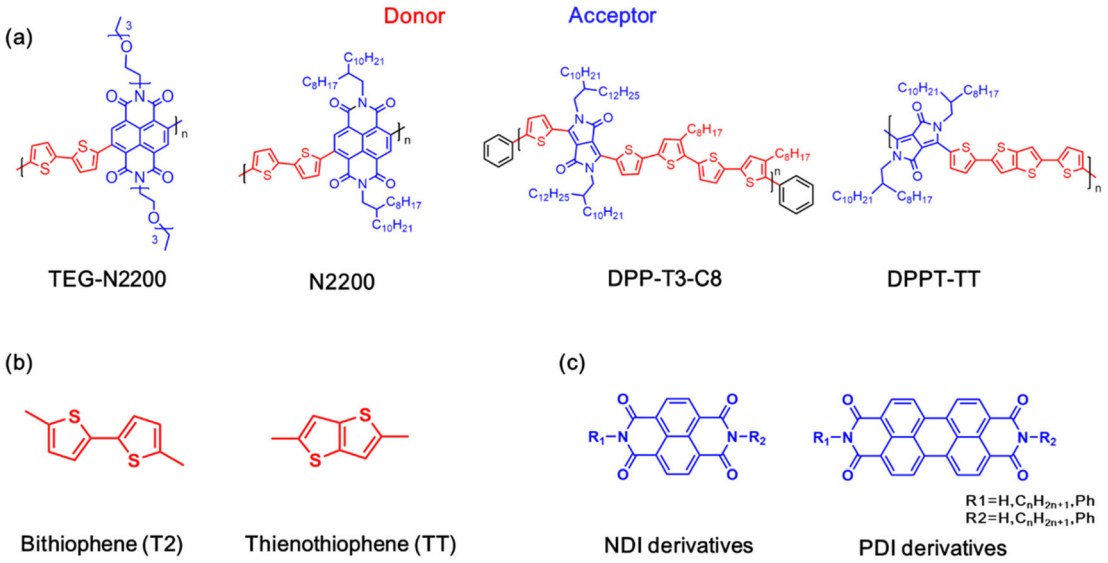

Fig. 2 (a) Structure of some donor–acceptor polymers commonly used for thermoelectrics (red: donor, blue: acceptor). (b) The building block used as an acceptor is a diimide (DI) derivative. (c) The donor moiety is a thiophene derivative.

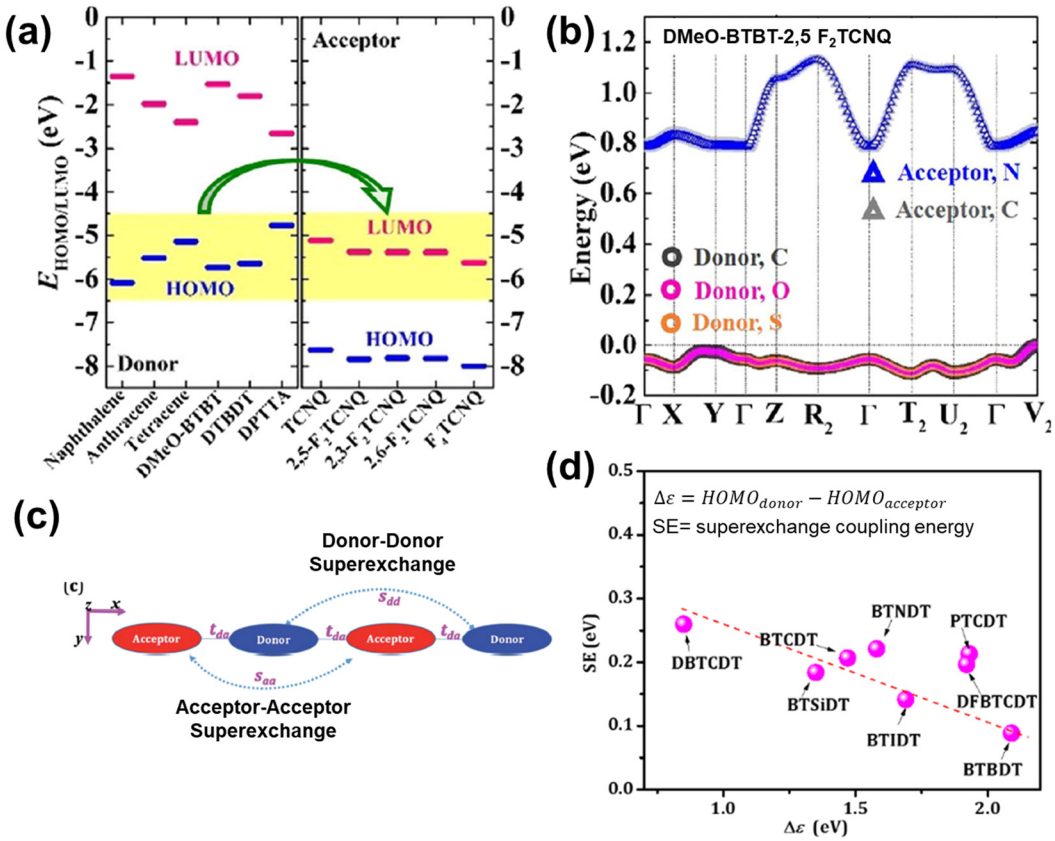

Fig. 3 (a) Charge transfer occurs from the higher energy HOMO level of the donor to the lower energy LUMO level of the acceptor. (b) An example of the resulting band structure on charge transfer: the donor forms the valence band, whereas the acceptor contributes to the conduction band[28] (reproduced with permission, copyright 2019, Springer Nature). (c) Schematic showing the donor–donor/acceptor–acceptor super-exchange coupling, which favors carrier delocalization, resulting in high carrier mobility. (d) The difference between the HOMO levels of the donor and acceptor ($\Delta\varepsilon$) should be minimized to obtain maximum super-exchange coupling energy (SE)[31] (reproduced with permission, copyright 2020, The Royal Society of Chemistry).

band structure. The orbital projected band structure of DMeO-BTBT as donor and 2,5-F_2TCNQ as acceptor in Fig. 3(b) clearly shows that the resulting charge transfer complex is a semiconductor where the energy states of the acceptor form the conduction bands, whereas the energy states of the donor form the valence bands. Although metallic behavior is not suitable for thermoelectrics, a small gap of <1 eV is ideal.[29,30] Hence, donor–acceptor combinations need to be chosen where the donor HOMO level is slightly lower than the acceptor LUMO level.

Although the intuitive push–pull effect due to the electron affinity difference between the donor and acceptor moieties is used to classically explain the transport of electrons in donor–acceptor polymers, a quantum description that accounts for donor to donor (or acceptor to acceptor) tunneling is required to account for charge transport through bands. Quantum mechanical super-exchange coupling can explain hole transport from donor to donor and electron transport from acceptor to acceptor[31] (Fig. 3(c)). The super-exchange coupling energy was evaluated from density functional theory-tight binding (DFTB) calculations by assuming that the charges are delocalized up to the second nearest neighbor, from donor to donor or acceptor to acceptor. From the DFTB calculations, it was observed that the increase in super-exchange coupling energy reduces the hole effective mass, m_0^* and the deformation potential, weakening electron–phonon coupling (Fig. 3(d)). This results in high carrier mobilities, which can potentially lead to high thermoelectric power factors. Fig. 3(d) shows that lowering the difference between the HOMO levels of the donor and acceptor ($\Delta\varepsilon$) increases the energy of the super-exchange coupling. Therefore, it is imperative to select donor–acceptor combinations such that the HOMO levels of the donor and acceptors become almost degenerate after the charge transfer process to achieve maximum mobility.

4. Tuning thermoelectric properties by molecular design

4.1 Changing aromatic ring constituents and donor–acceptor sequence to maintain high *S* and σ

It is well known that sharp density of states (DOS) is ideal for thermoelectrics as it can potentially achieve both high electrical σ and *S*.[32] Sharp DOS favors degeneracy at lower carrier concentrations, potentially leading to a high concentration of states around the E_F, which can result in high σ.[33] Thus, even at moderate carrier concentration, it can give high σ, which will aid in retaining a high *S* by maintaining an asymmetry in the number of conducting states above and below E_F. Hence, the objective should be to make the DOS narrower by modifications of the chemical structure. Liu *et al.*[34] have recently shown that embedding sp^2-hybridized N atoms in the donor moiety (replacing a sp^2-hybridized C with a sp^2-N) narrows down the DOS of a donor–acceptor polymer, which results in a high *S* and σ (Fig. 4(a)). Additionally, the embedding of the N-atoms increases the backbone planarity. The planar backbone facilitates the ordered stacking of chains, thereby enhancing crystallinity and interchain charge transport. Therefore, altering the molecular structure by embedding the N-atoms enhances both inter and intrachain transport. An alternative way to think about this, although not directly mentioned by the study in context, is that the narrowing of the DOS results from of the decreasing disorder in the system caused by increased planarity of the backbone, as the disorder-to-order transitions make the energy levels more degenerate.

Usually, conjugated polymers are either a sequence of donor molecules or acceptor molecules and, when doped, result in a high σ but a low *S*.[35,36] In the case of the donor–acceptor polymers, the acceptor repels p-type dopants, whereas the donor repels n-type dopants due to opposite charges, resulting in reduced doping efficiency.[22,37] This results in a high *S* but low σ. Recently, an innovative approach of random copolymerization to generate a random sequence of donor and acceptor moieties demonstrated both high *S* and σ.[21] As shown in Fig. 4(b), the random copolymerization results in three-dimensional zones of donors separated by zones of acceptors. This leads to more efficient doping of the donors and enhances mobility by facilitating the hopping of charges from electron-pushing donor regions and electron-pulling acceptor regions. This is analogous to the concept of modulation doping for inorganics, where nanograins of a doped semiconductor were embedded into another semiconducting matrix such that the carrier from the nanograins spills over to the undoped host.[38] This significantly enhanced charge mobility by reducing scattering from ionized dopant impurities. High mobility ensures the attainment of a high σ with minimal extent of doping. This helps in retaining a high *S* while maintaining a high σ.

4.2 Open-shell backbone offers high intrachain mobility

In the ground state, most polymers have paired electrons in the singlet state with spin quantum number $s = 0$ with a closed-shell structure.[39] In most cases, thermal transitions from singlet to doublet ($s = 1/2$) and triplet ($s = 1$) states are energetically unfavorable. However, for several donor and acceptor moieties, the existence of an open-shell structure as radicals (doublet) and diradicals (triplet) in the ground state is energetically favorable even at room temperature. An open-shell structure or the presence of radicals and diradicals along the polymer backbone increases the intrinsic intrachain σ. Donor–acceptor polymers with triplet ground state can have an intrinsic σ of $\sim 10^{-2}$ S cm^{-1}.[40] The high intrinsic σ requires the minimum usage of dopants, which is very advantageous, as excessive use of dopants can greatly reduce mobility by localization or scattering. Having the open-shell configuration has the same effect as moderate doping, and thus, polymers with diradicals are often termed self-doped semiconductors.[41–43] Additionally, the use of open-shell dopants with open-shell polymers has been proven to be an effective strategy to achieve a 100× increase in σ.[44,45] This is because open-shell moieties are devoid of ions, which localize carriers *via* coulombic interactions.

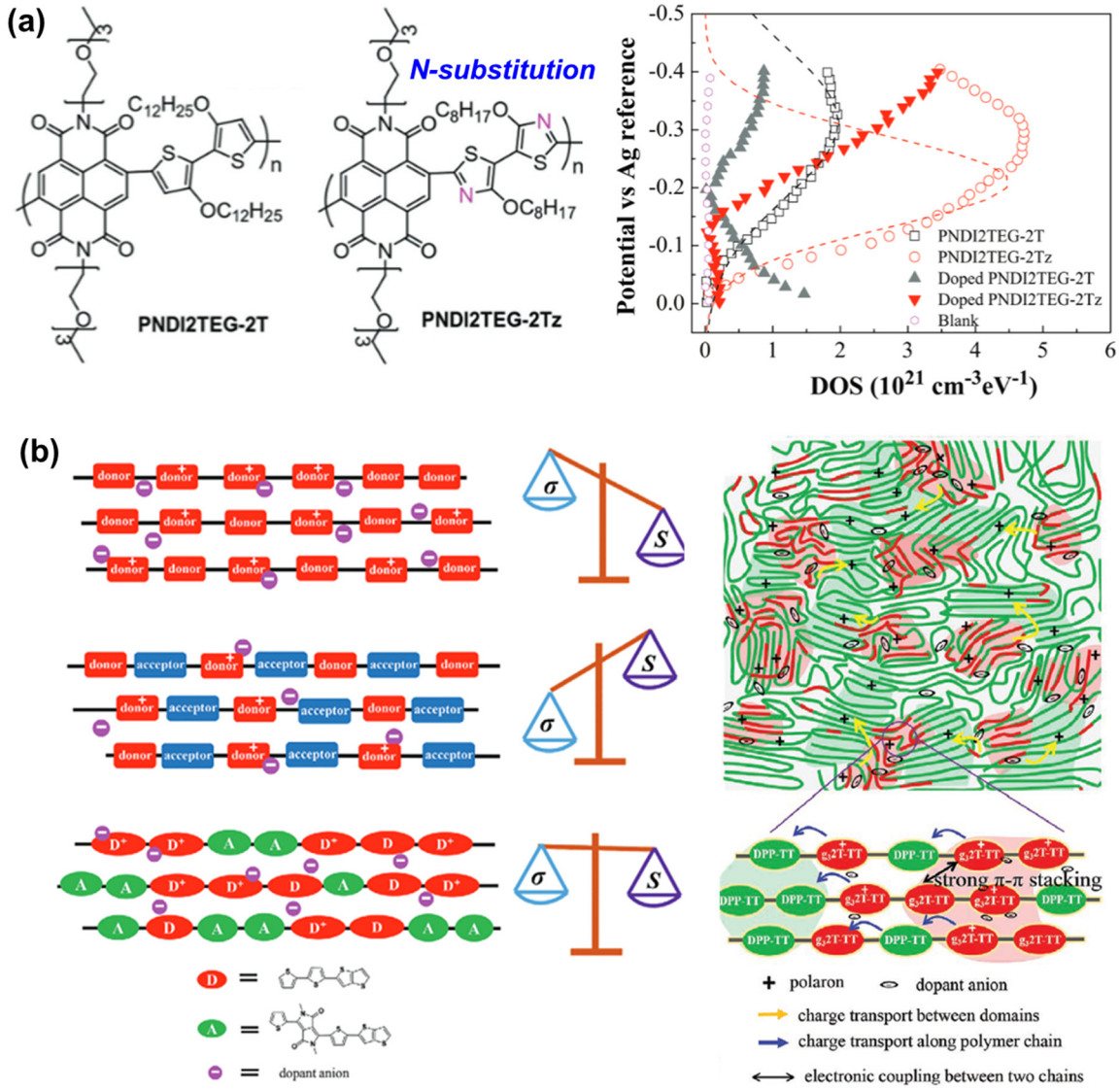

Fig. 4 (a) sp^2 N-substitution in the donor moiety makes the DOS of the donor–acceptor copolymer narrower (degenerate), which is ideal for maintaining a high σ and S[34] (reproduced with permission, Copyright 2018, Wiley-VCH). (b) Polymers with only donors have a high σ and low S, polymers with an alternate sequence of donors and acceptors have a high S due to interchain energetic disorder but low σ, whereas polymers with a random sequence of donors and acceptors have both high S and σ[21] (reproduced with permission, copyright 2020, Wiley-VCH).

The singlet and triplet states are the resonant structures of the same molecule, but the selectivity of the triplet states is usually lower owing to their high energy. Hence, lowering the energy difference between the singlet and triplet state (ΔE_{S-T}) increases the stability of the triplet state. A recent study[44] has shown that copolymerization of building blocks with low ΔE_{S-T} results in a low ΔE_{S-T} or a high diradical character of the donor–acceptor polymer obtained from the copolymerization process. Fig. 5(a) shows the ΔE_{S-T} of fused aromatics as acceptor units used as building blocks of donor–acceptor polymers. The decreasing ΔE_{S-T} increases the stability of the open-shell structure. Hence, the use of building blocks with stable triplet ground states can be an effective strategy in the development of donor–acceptor polymers with high mobility and σ, without sacrificing S. Although the energetics of the building blocks ensure the stability of the triplet ground state of the copolymer, high spin densities (high concentration of diradicals) in the solid state may lead to interchain spin interactions and cancellation due to disordered alignment of chains, which can result in the reduction of triplet state (s = 1) to doublet state (s = 1/2). This will not happen at low spin densities where the interactions of the spins are limited to intrachain.

Recent studies have shown that stabilizing triplet ground states through the use of strongly proquinoidal donor and acceptor units can significantly enhance the intrinsic charge transport properties of donor–acceptor polymers. Donor–acceptor backbones with extended π-delocalization and narrow singlet–triplet energy gaps have been demonstrated to exhibit

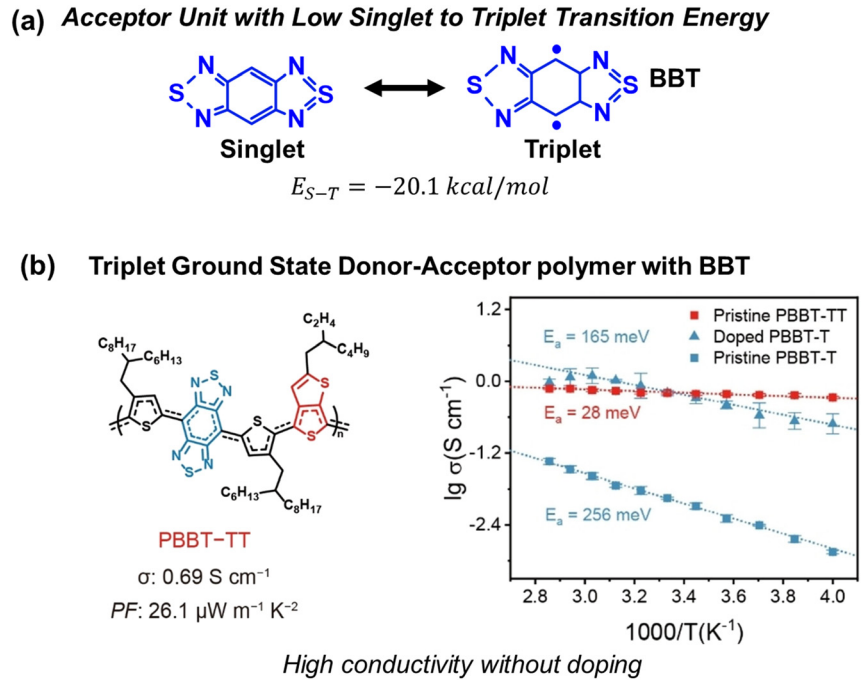

Fig. 5 (a) Singlet and triplet states of a common acceptor BBT. (b) A triplet ground state stabilized donor–acceptor polymer with BBT almost shows the same conductivity as a doped polymer and orders of magnitude higher conductivity than intrinsic semiconducting polymers (reproduced with permission, copyright 2024, Wiley-VCH).[46]

high electrical conductivities in the undoped state, reaching values above 8 S cm^{-1}. Moreover, polymers designed with near-pure diradical character and enhanced spin density distribution have achieved power factors exceeding 25 μW m^{-1} K^{-2}, while maintaining ambient stability.[46] The conductivity of the intrinsic triplet-state stabilized polymer PBBT-TT almost matched the conductivity of a doped singlet-state polymer and have order of magnitude higher value than intrinsic singlet-state polymers (Fig. 5(b)). These findings highlight that tuning of molecular structure through backbone rigidity, spin delocalization, and controlled electronic coupling, can simultaneously promote σ and S, offering the path to high-performance thermoelectric materials without the need for external dopants or with minimal dopant concentrations. However, it should be noted that open-shell structures are inherently prone to oxidation, and their stability must therefore be carefully evaluated in future studies aimed at device development.

4.3 Backbone and sidechain modification to facilitate interchain transport

Using the inductive effect of side chains to enhance doping efficiency is an effective strategy for doping any semiconducting polymer. For semiconducting polymers, p-type doping involves the oxidation of a particular site, generally sulfur (S), whereas n-type doping involves the reduction of a specific type, which is usually a π-bonded carbon (C). In the case of p-type doping, alkyl groups with a positive inductive effect have been effective in pushing electrons to the oxidation site (S), thereby lowering the electron affinity of the doped polymer and enhancing the effectiveness of p-type doping.[47,48] Similarly, n-type doping, halogen (F, Cl, *etc.*) containing functional groups that have a negative inductive effect increases the electron affinity of the doped molecule by removing electrons from the reduction site (C), hence enhancing the n-type doping efficiency (Fig. 6(a)).[22] Additionally, the incorporation of highly polar halogenated functional groups induces attractive intermolecular interactions between the polymer chains as well as between the polymer chains and the dopants.[49,50] Also, the fluorinated groups are thought to have intrachain H-bonding, which reduces the rotational degrees of freedom, thereby leading to a more ordered structure.[22] This results in better packing and alignment of the polymer chains and increases the miscibility of the polymer with the dopant (Fig. 6(b)). The strong intermolecular interactions and closer packing increase order (crystallinity) in the system and facilitate extended conjugation and band-like transport, leading to high interchain mobility. The doping reaction may not be limited only by energetics but can also have mass transfer limitations, which will depend on the proximity of the polymer chains to the dopant. Hence, better miscibility of the dopant with the polymer can enhance the kinetics of the doping reaction by removing mass transfer limitations.

Although donor–acceptor polymers have the potential to offer high intrachain mobility, the overall transport, like other organic systems, is still limited by the interchain hopping of charges caused by localized states due to a lack of long-range order in three dimensions.[20,51,52] A coplanar backbone not only aids the intrachain delocalization of the charge cloud but

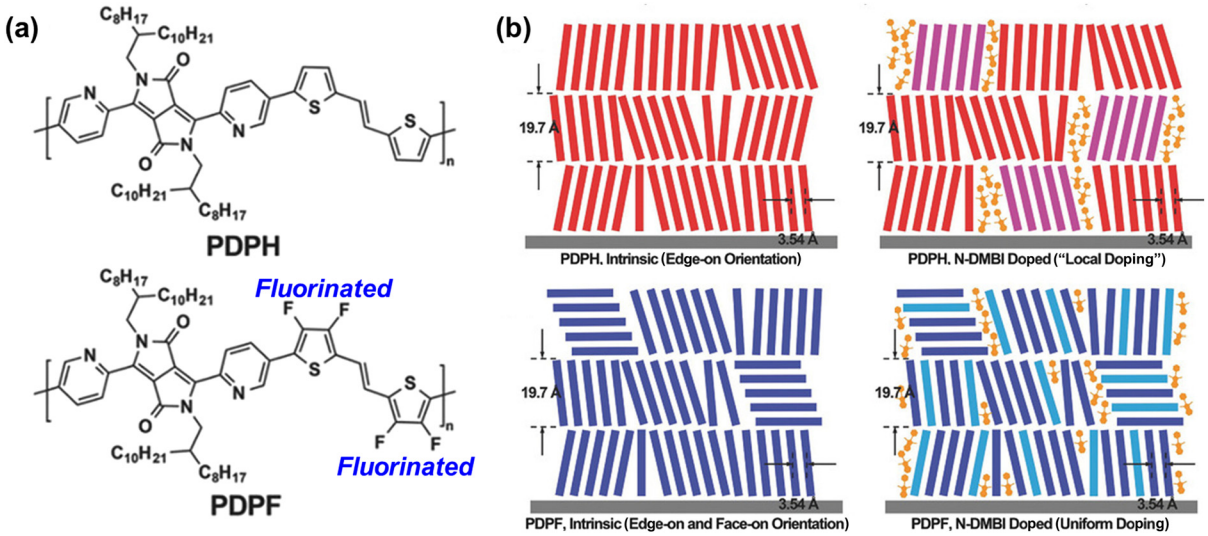

Fig. 6 (a) Incorporation of F as an electron-withdrawing group on the donor increases the electron affinity of the donor–acceptor copolymer, thereby improving n-type doping efficiency. (b) The polar C–F groups also increase the interchain, intrachain, and chain-dopant attractive interactions, reducing disorder in polymer structure and enhancing the miscibility of the polymer and dopant, resulting in more uniform doping[22] (reproduced with permission, copyright 2018, Wiley-VCH).

also enhances the interchain packing and alignment by increasing the extent of π–π stacking. π–π stacking causes the interchain delocalization of the charge carriers (polarons and bipolarons), promoting band-like transport, which can improve the σ by orders of magnitude.[53–56] Prior work[57] has shown that the replacement of thiophenes with thiazoles (Fig. 7(a)) as the donor moiety ensures a more planar backbone, which also results in better packing between the polymer chains. The thiazoles restrict the rotational degrees of freedom (Fig. 7(b)), thereby preventing random coiling and bending of the chains, which makes the system more ordered. The introduction of more orders ensures higher carrier mobility. On doping, the S almost remains unchanged between the thiazole and the thiophene, but the carrier mobility and the σ drastically increase. This causes the thiazole-substituted system to possess a ~1000× higher power factor, as shown in Fig. 8(c) where t_{vapor} represents the time of exposure of the polymers to the dopant (tetrakis(dimethylamino)ethylene/TDAE) vapor.

5. Tuning thermoelectric properties *via* mesostructures

Apart from inducing intermolecular interactions by chemical modifications, physical parameters can be tuned during the fabrication process to control the crystallinity and mesostructural order of donor–acceptor polymer films. It is well established that electrons undergoing band transport are scattered by grain boundaries, or there is a transition from band to hopping transport, resulting in a depreciation of σ.[62–64] Hence, bigger grain sizes have higher σ. Another study[58] followed a kinetically controlled crystallization (KCC) method to grow P(NDI2OE-T2) films by regulating the solidification rate of the film after spin-coating (Fig. 8(a)). As expected, a slower solidification rate at a lower temperature led to higher crystallinity and bigger grain sizes, which led to a mobility enhancement of 100×.

Another way to induce crystallinity and order is by dimensional confinement. A self-seeded growth method was employed for synthesizing nanofibrils of P3HT.[59] Needle-like seeds of P3HT were initially dispersed in the solution phase, and temperature-controlled nucleation of P3HT was performed on the dispersed 1-D seeds, which led to the growth of highly crystalline 1-D nanofibrils of P3HT (Fig. 8(b)). The increased crystallinity and alignment by 1-D confinement is expected to significantly enhance carrier mobility. The same approach can be followed for donor–acceptor polymers.

Polymers solidify as spherulites, which contain highly crystalline zones with completely aligned chains separated by disordered amorphous zones. Mechanical drawing of polymers has been traditionally used to align polymer chains and increase the crystallinity of polymer films.[65–68] The drawing process is usually conducted above the glass transition temperature of the polymers, beyond which the polymer chains can move freely on stretching and relax at equilibrium positions, forming a highly ordered structure. Recently, a study[60] uniaxially stretched a doped P3HT film, as shown in Fig. 8(c), with a DMA instrument with a draw ratio of 4 and obtained a ~40× higher σ with an almost unchanged S along the drawing direction. High-temperature rubbing is another mechanical process used to improve the surface alignment of conjugated polymer chains on the sample surface. The rubbing motion introduces a shear on the surface of the deposited film that enhances the alignment of polymer chains. Another study[61] rubbed P(NDI2OD-T2) thin film in one direction, applying constant

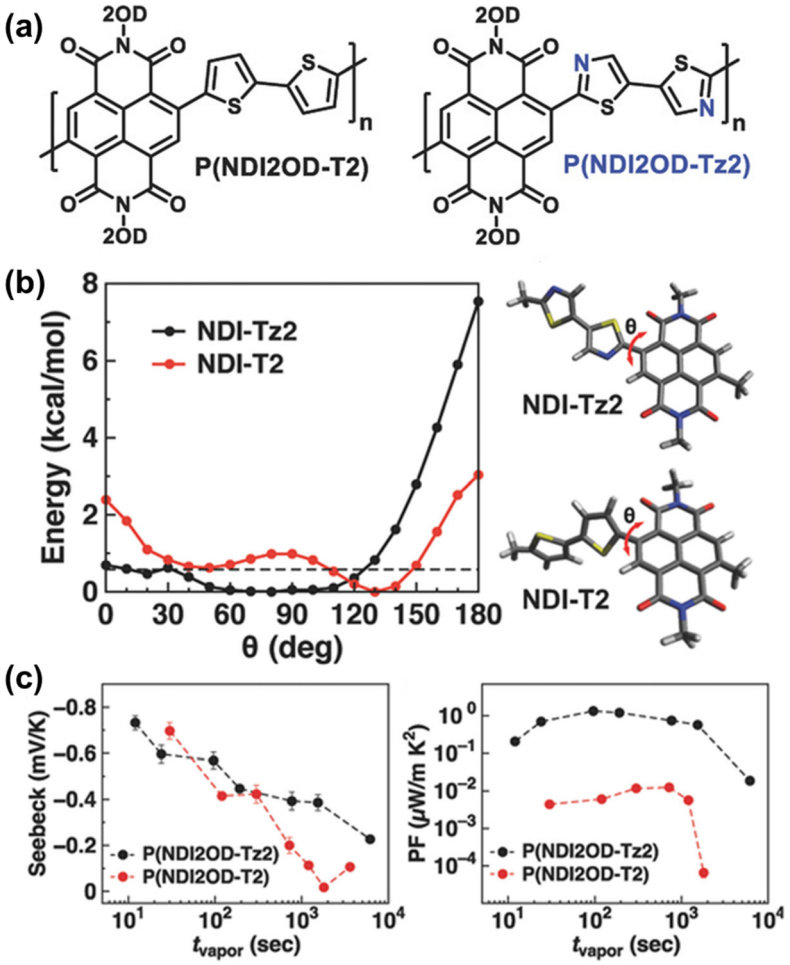

Fig. 7 (a) Replacement of thiophenes with thiazoles as donor moiety. (b) Thiazole poses a higher energy barrier to rotation, thereby restricting the random coiling of the chains, which ensures more order in the system and improves interchain carrier mobility. (c) The thiazole-substituted chain has the same *S* as that of the thiophene but possesses a ~1000× higher power factor[57] (reproduced with permission, copyright 2020, Wiley-VCH).

pressure by a rotating cylinder while annealing at a high temperature, and obtained a film with highly aligned chains (Fig. 8(d)). The carrier mobility along the rubbing direction went up by ~5×.

6. Effect of dopants

6.1 Thermodynamic limitations on doping efficiency

Donor–acceptor polymers offer the advantage of being doped as both n-type and p-type. Prior work on organic thermoelectrics has mainly focused on p-type conjugated polymers, such as PEDOT:PSS. Similarly, p-dopants have been mostly explored for donor–acceptor polymers, and very few studies exist on n-doped donor–acceptor polymers. Moreover, the best charge transport properties and thermoelectric performances have been reported for p-type polymers that outperform the n-type polymers by orders of magnitude.[69,70] Molecular doping differs significantly from substitutional atomic doping in inorganics. In inorganics, both dopant and semiconductor lattice are neutral at the ground state, whereas in the case of molecular doping, a ground state charge transfer complex (CTC) is formed by electron exchange between the dopant and the semiconductor.[71] Hence, for p-type molecular doping, the neutral dopant LUMO needs to be lower than the neutral host HOMO so that an electron is transferred from the semiconductor host to the dopant to form the CTC. For n-doping, the neutral dopant HOMO needs to be higher than the neutral host LUMO at the ground state so that an electron is transferred from the dopant to the semiconductor host to form the CTC. This leads to the formation of two gap states, out of which one is localized on the semiconductor and the other on the dopant. However, carriers in the semiconductor gap state are bound to the opposite charges in the dopant state, which must acquire thermal energy to overcome the coulombic binding energy and hop into the extended bands to participate in transport.[71] The inferior performance of the n-type polymers is due to the poor doping efficiency and stability of the n-type dopants under standard atmospheric conditions. This is an inherent challenge for n-type dopants as they have high

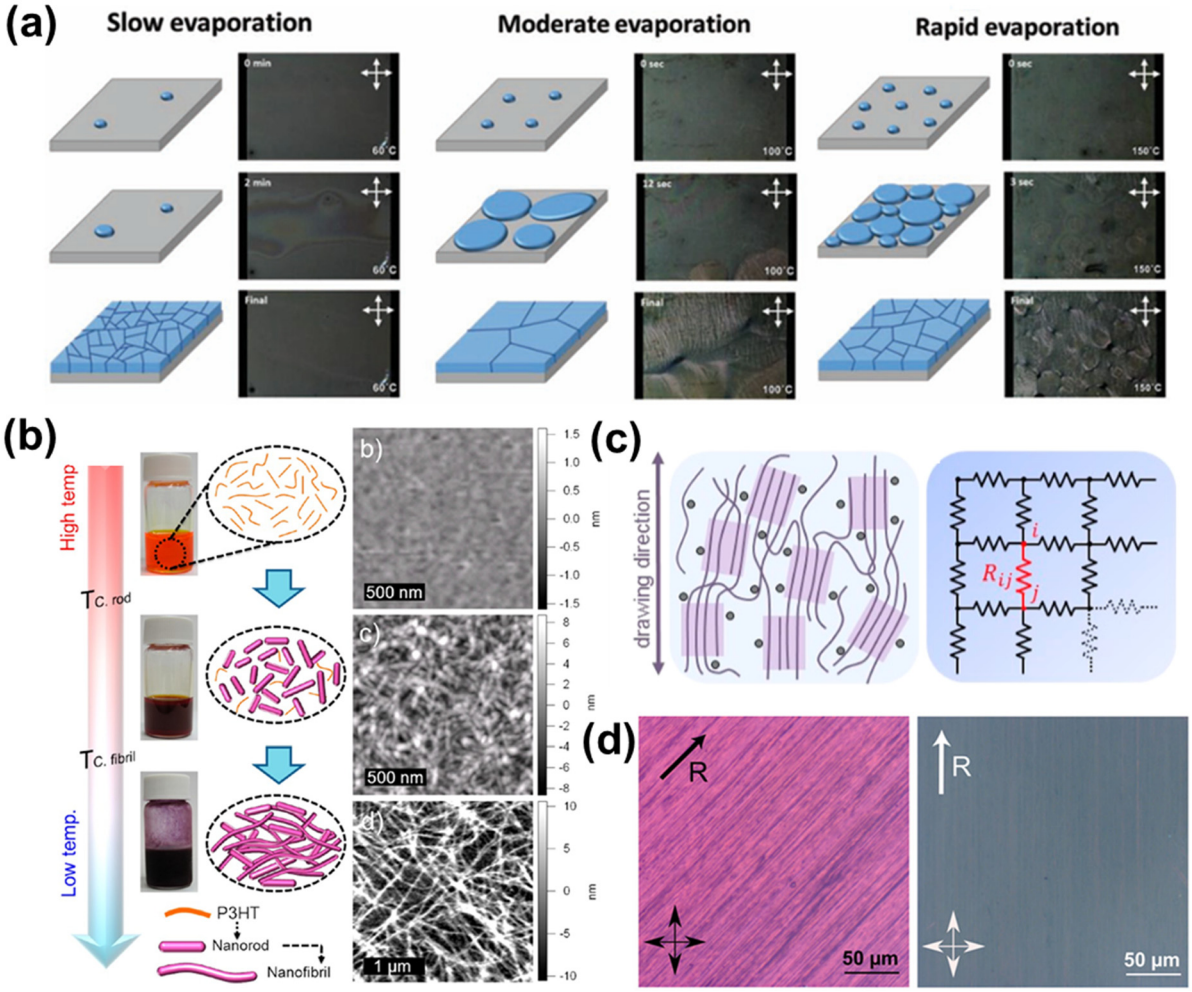

Fig. 8 (a) Controlling crystallite size kinetically by controlling evaporation-driven solidification rate[58] (reproduced with permission, copyright 2019, Wiley-VCH). (b) Nucleating on 1-D seeds leads to spatial confinement and the formation of highly crystalline polymer nanofibrils[59] (reproduced with permission, copyright 2012, American Chemical Society) (c) mechanical drawing induces crystallinity by aligning polymer chains and creating an ordered network of resistors with high carrier mobility[60] (reproduced with permission, copyright 2019, American Chemical Society) (d) highly aligned chains are obtained by mechanical rubbing at the glass transition temperature[61] (reproduced with permission, copyright 2019, Wiley-VCH).

HOMO levels and are more likely to transfer electrons to oxygen or moisture, which have a much deeper LUMO level than that of the semiconducting polymers (Fig. 9(a)).[72] The most widely used n-type dopant is N-DMBI-H because it is relatively air-stable owing to its low HOMO level. However, it suffers from poor doping efficiency as its HOMO level is lower than most of the organic semiconductors.[73]

The doping through N-DMBI-H occurs either *via* (i) a hydride ion (H^-) transfer process from the N-DMBI to the doped molecule (ii) a free-radical pathway: N-DMBI-H → N-DMBI$^\bullet$ + H$^\bullet$, and the free radical transfer the electrons to the doped molecule.[73] As shown in Fig. 9(b), the HOMO level of N-DMBI is lower than the LUMO of both the polymers, A (A-DCV-DPPTT) and Q (A-DCM-DPPTT). However, when it is activated to the free radical state, the singly occupied molecular orbital (SOMO) of the free radical has a higher energy than the LUMO of both polymers, which results in successful n-doping. However, the activation energy of both the free-radical generation (80.2 kcal mol^{-1}–335 kJ mol^{-1}) and the hydride transfer (74.6 kcal mol^{-1}–312 kJ mol^{-1}) are very high (Fig. 9(c)), resulting in slow kinetics of the doping reaction thereby limiting the doping efficiency.

A recent study[74] employed a layer of gold nanoparticles as a catalyst bed between the glass substrate and a spin-coated film of blended perylene diimide (PDI) based polymer and dopant (N-DMBI-H). Gold as a transition metal catalyst reduces the activation barrier of the lysis of the C–H bond of N-DMBI-H by ~32 kcal mol^{-1} (~133 kJ mol^{-1}), thereby facilitating the doping process involving hydride ion transfer from N-DMBI-H to PDI, as shown in Fig. 9(d). Thus, using a bed of transition metal catalysts is a simple and effective strategy for the development of stable n-type devices from any organic semiconductors. While this catalytic strategy provides a practical

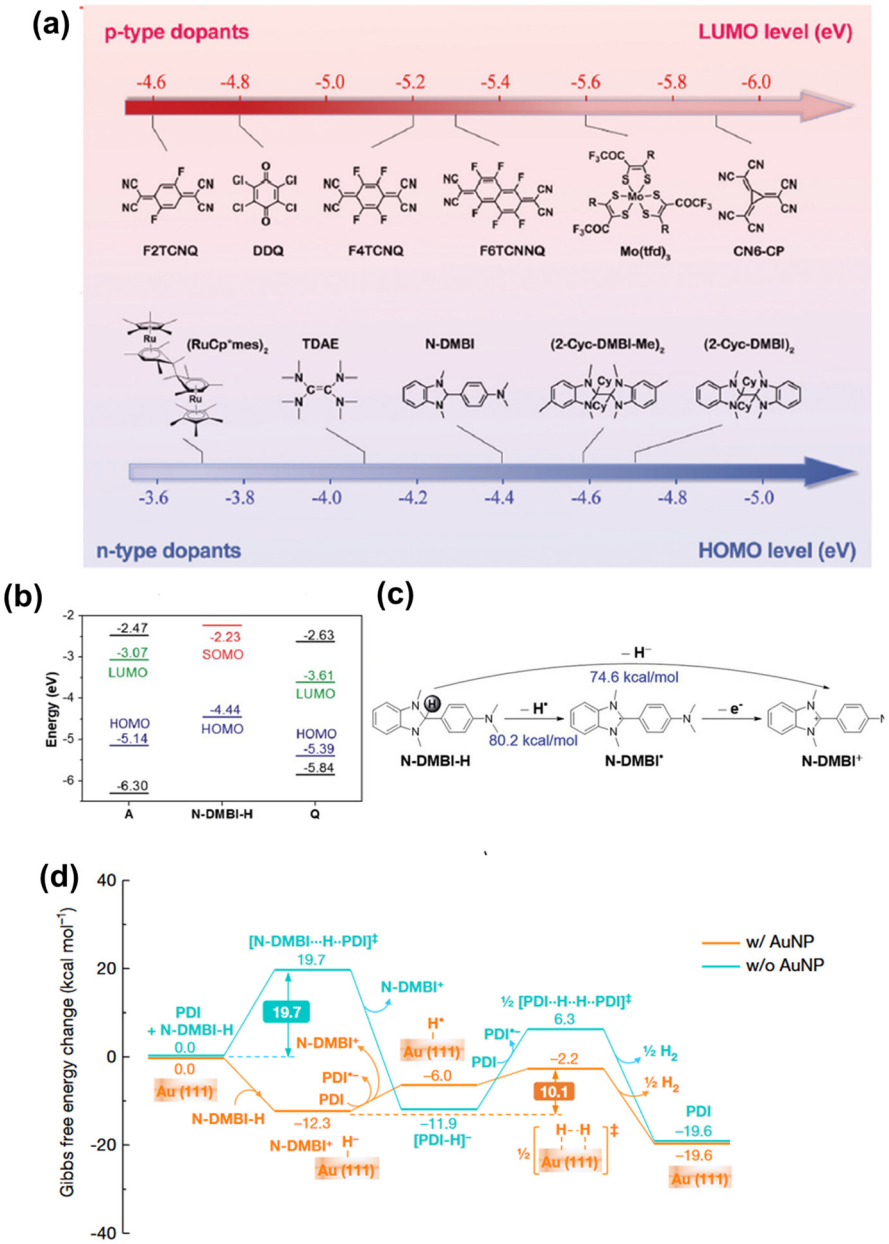

Fig. 9 (a) Energy levels of different p-type and n-type dopants used for organic semiconductors in general. N-type dopants are relatively unstable in the air as their high HOMO levels cause them to transfer electrons to oxygen/moisture instead of the doped polymer[72] (reproduced with permission, copyright 2020, The Royal Society of Chemistry). (b) Air-stable dopant N-DMBI-H has a lower HOMO level than the LUMO level of the polymers A (A-DCV-DPPTT) and Q (A-DCM-DPPTT), but it forms a free radical as an intermediate which has a SOMO level higher than the LUMO level of both polymers. (c) Both possible doping pathways followed by N-DMBI-H, through free radical formation and through hydride ion transfer, have high activation energies[73] (reproduced with permission, copyright 2020, The Royal Society of Chemistry). (d) The activation energy of the doping reaction can be lowered by depositing a layer of AuNPs as catalysts between the spin-coated polymer-dopant blend and the substrate[74] (reproduced with permission, copyright 2021, Springer Nature).

route to improve the reactivity of existing dopants, recent advances have taken alternative approaches to overcome the intrinsic limitations of conventional n-dopants like N-DMBI-H. One such approach utilizes photoactivable dopants that undergo UV-triggered conversion into active hydride donors, enabling spatially resolved n-doping down to 1 μm and achieving conductivities as high as 31 S cm^{-1} without requiring thermal activation. In parallel, thermally activated triaminomethane-type dopants, designed through DFT-guided screening, exhibit high doping efficiency, exceptional air and solution stability, and excellent miscibility with polymer side chains. Triaminomethane-type dopants achieves conductivities up to 21 S cm^{-1} and thermoelectric power factors of 51 μW $m^{-1}·K^{-2}$ in thick (>10 μm) films while preserving polymer mor-

phology. These new classes of dopants illustrate how molecular doping barrier can be overcome catalytically or through photo/thermal-activation, enabling stable, high-performance n-type doping in donor–acceptor polymers.[75,76]

6.2 Charge localization by dopants limits mobility

The strong coulombic binding energy of the dopants, limits charge transport in most conjugated polymers. The dopants are bonded to the polymers, and the highly polar character of the strong bonds increases the coulombic binding energy, thereby localizing charges, as mentioned in Section 4. Strong localization effects of PSS as a dopant for PEDOT have been observed due to ionic bonding between the PEDOT and PSS.[77–79] $FeCl_3$ as a dopant also causes a significant extent of charge localization in P3HT.[80,81] Although dopants increase carrier concentration, dopants with high binding energy with the host significantly affect mobility by charge localization. A couple of prior work[37] has followed the strategy of replacing a small dopant such as $FeCl_3$ with a bulky dopant such as Tris (pentafluorophenyl) borane (BCF), such that the steric interactions between the polymer side chains and the bulky functional groups of the dopant results in lowering of the binding energy of the dopant with the polymer (Fig. 10). The weak coulombic binding energy results in enhanced transport and high σ. Hence, the dopant structure should be modified to optimize the electron affinity of the dopant and the bond strength between the dopant and polymer to facilitate charge delocalization along the polymer backbone. However, bulky dopants can introduce excluded volume and may have lower miscibility with the polymers. This will decrease the doping efficiency as well as lower the gravimetric thermoelectric energy conversion efficiency. Hence, one has to find a balance between the size of the dopant and the binding energy of the dopant with the polymer.

7. Path forward

7.1 Decoupling seebeck from electrical conductivity

We curated S and σ from various sources and represented their correlation in Fig. 11. S decreases with σ as expected. The inverse relationship implies that the σ enhancement in most of the studies resulted from an increase in carrier concentration which decreased S. High mobility due to inherent structure or mobility enhancement by structural changes,

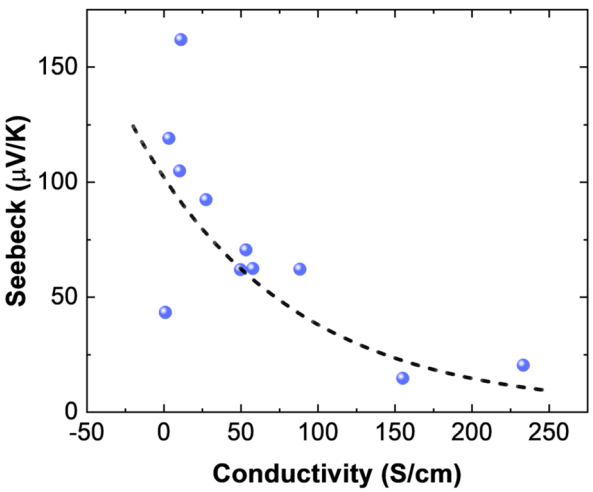

Fig. 11 Data curated from various sources[37,82–86] by us suggest that S and σ are still inversely coupled for donor–acceptor polymers.

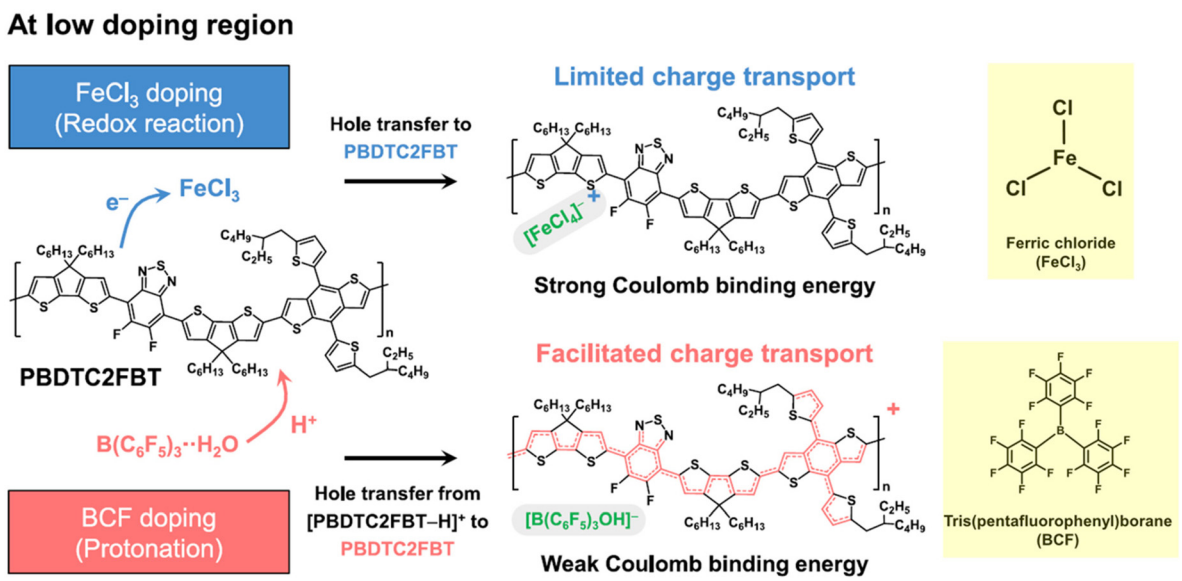

Fig. 10 $FeCl_3$ as a dopant has a strong coulomb binding energy with the polymer, which results in the localization of charges. Bulky dopant BCF has a weaker coulombic binding energy with the polymer, which prevents charge localization and facilitates charge transport[37] (reproduced with permission, copyright 2024, American Chemical Society).

instead of doping, is desirable to maintain a high S and high σ, as doping increases the chemical potential of the electrons, thereby reducing S. As mentioned in the review, structural modifications such as sidechain and backbone engineering to promote interchain π–π stacking, stabilizing triplet states of the donor–acceptor moieties, randomly sequencing the donor and acceptor moieties, and physical alignment of chains by slow crystallization and stretching can collectively enhance the carrier mobility, such that minimal extent of doping is required to achieve a high σ while retaining a high S. Although this review summarizes the important factors controlling the properties of donor–acceptor polymers, further mechanistic exploration is required to completely understand the complex structure–function relationships. Additionally, because of disorder, molecular systems like donor–acceptor polymers have Gaussian DOS. Hence, the relationship between their S and σ should differ significantly from that of parabolic semiconductors. Decoupling S from σ can bring a paradigm shift in thermoelectrics research as it will potentially push the thermoelectric power factor several times beyond the currently existing best-performing thermoelectric materials. However, the mechanisms behind the decoupling of these parameters have not been established. As molecular systems have differently shaped DOS than inorganic semiconductors, the relationship between S from σ in these systems needs to be clearly understood, and the possibility of decoupling these two parameters needs to be further explored.

7.2 Accurate mobility measurement

In traditional inorganic semiconductors, carrier mobility and concentration are usually estimated from Hall effect measurements by assuming that the carrier concentration and the mobility are independent of each other,[87–89] which can be invalid for organic semiconductors due to the following two reasons. Primarily, the coulombic energy of the dopants localizes charge carriers. However, with increasing extent of doping additional carriers screen these interactions, leading to charge delocalization and a corresponding increase in mobility. Thus, increasing carrier concentration increases mobility and they are not independent. Secondarily, introducing molecular dopants always changes the polymer structure and, in turn, changes the mobility. These make the mobility dependent on the carrier concentration. Hence, alternative methods to characterize the charge carrier concentration need to be explored.

Recent work[90] has shown that nuclear magnetic resonance (NMR) peak shift can be used to estimate the carrier concentration independently in organic semiconductors. The carrier concentration induced by an F-containing dopant was estimated by characterizing the peak shift in ^{19}F NMR (Fig. 13(a)). The shift was calibrated with different concentrations of dopants. Simultaneously, the same samples with different concentrations of dopants were used for Vis-NIR absorption spectroscopy measurement to estimate the exciton bleach percentage (Fig. 13(a)). The carrier density was obtained by correlating the exciton bleach percentage with the NMR peak shift. The estimated n was used to calculate μ through $\sigma = ne\mu$ obtained from independent σ measurements. Another frequently used method that can provide an independent estimation of carrier mobility is the field effect transistor (FET) based time-of-flight method, where the time-of-flight of the charges injected by the electrodes is used to estimate the carrier mobility. Also, recent studies[91] have shown that the DOS near the HOMO and LUMO levels of organic semiconductors can be characterized by energy resolved-electrochemical impedance spectroscopy and can be used to estimate bandgap and carrier concentration (Fig. 13(b)).

7.3 Thermal conductivity characterization

In general, untreated polymers are disordered and have low thermal conductivity (k) ~0.2 W m^{-1} K^{-1}.[68,92–94] However, donor–acceptor polymers can potentially have a high k when (i) heavy doping makes σ ~10^3 S cm^{-1}, increasing electronic contribution to k and (ii) enhancing crystallinity by the aforementioned structural changes, which also increases lattice k.[95] The enhancement of the electronic contribution to the k has already been observed for the conjugated polymer PEDOT:PSS.[96] Usually, polymer films are dimensionally anisotropic, the thickness being much smaller than the length and width.[94,97–99] The confinement along the thickness (through-plane) causes preferential alignment of the chains along the in-plane direction, simultaneously reducing excluded volume effects in the in-plane direction. Therefore, both electrical carrier mobility and k will be higher along the in-plane direction,[100] as shown in Fig. 12(a). A study[96] found a positive linear correlation between the in-plane σ and k, as stated by the conventional Wiedemann-Franz law, with k reaching up to ~1 W m^{-1} K^{-1} (Fig. 12(b)). However, the through-plane k is much lower ~0.3 W m^{-1} K^{-1}, and independent of the in-plane σ. This suggests that the enhancement of k in the in-plane direction is a result of σ enhancement.

The donor–acceptor polymers have been mostly characterized for power factor enhancement. However, the actual figure of merit, $zT = \frac{S^2\sigma}{k}T$, can be significantly affected when k reaches a high value.[32,101,102] Different donor–acceptor polymers with different interchain interactions and high interchain electron mobility may have different degrees of anisotropy in k. Therefore, experimental and computational exploration of the in-plane k of donor–acceptor polymers and understanding the factors controlling their k is necessary.

7.4 Database development and machine learning

ML algorithms can analyze vast datasets of polymer structures, electronic properties, and thermoelectric performance metrics to identify patterns and predict optimal donor–acceptor combinations for enhanced charge mobility, S coefficient, and k.[103,104] Hence, a database on energetics and structure–property relationships needs to be generated first.[105–107] With ML, one can design novel polymer backbones by exploring untapped chemical spaces and suggesting innovative structures with tailored bandgaps and doping efficiencies. The database and ML model will be specifically useful for selecting

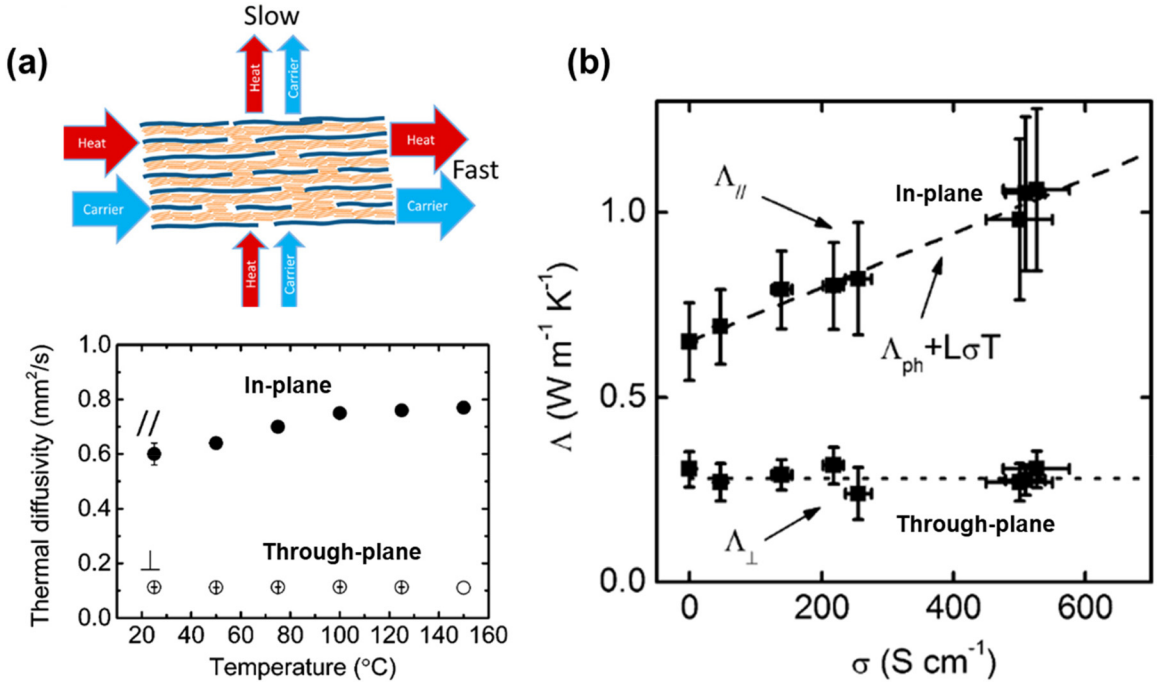

Fig. 12 Anisotropic thermal conductivity of conjugated polymer (PEDOT:PSS) dominated by electronic contribution from independent studies (a)[100] and (b)[62] (reproduced with permission, copyright 2012 and 2014, American Chemical Society).

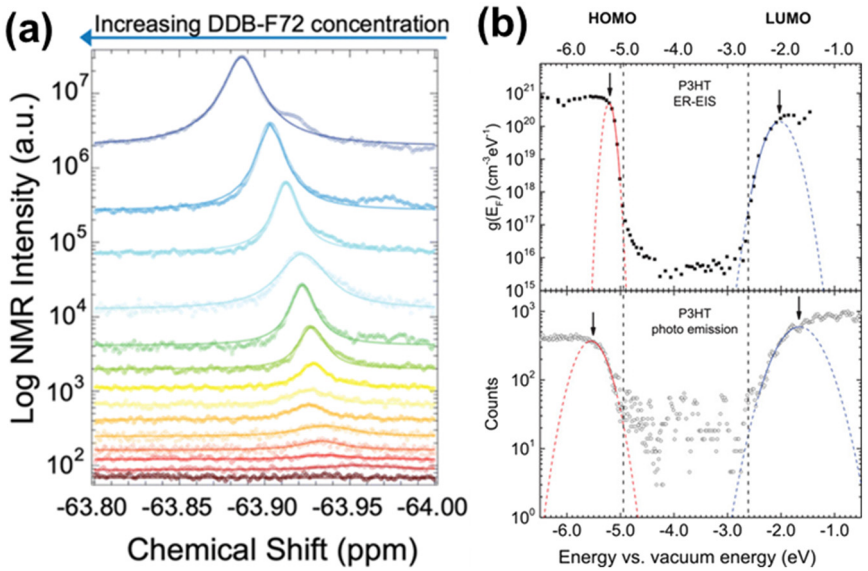

Fig. 13 (a) Carrier concentration from NMR peak shift[90] (reproduced with permission, copyright 2024, The Royal Society of Chemistry) (b) DOS from energy resolved-electrochemical impedance spectroscopy and photoemission spectroscopy[91] (reproduced with permission, copyright 2021, Wiley-VCH).

donor–acceptor combinations to develop organic semiconductors with a wide range of bandgaps. This will not only be useful for thermoelectrics, rather, it will be attractive to all communities interested in bandgap modulation of semiconducting polymers, including photovoltaics. Additionally, ML models can accelerate experimental workflows by guiding synthesis priorities and reducing trial-and-error processes. These tools can also improve understanding of structure–property relationships, allowing researchers to fine-tune morphology, crystallinity, and doping strategies for better thermoelectric efficiency. Fig. 14 shows how such predictive modeling has been used for designing small-molecule semiconductors.

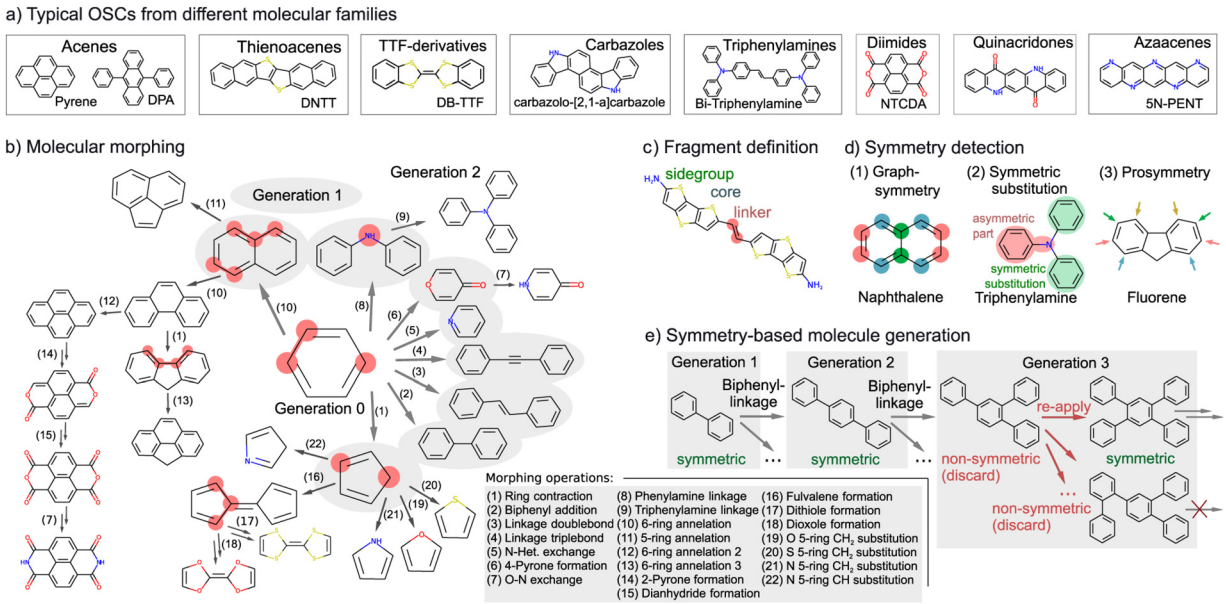

Fig. 14 Molecular construction approach to generate an unlimited small molecule organic semiconductor chemical space. Such approaches to extend the chemical space of donor–acceptor polymers may bring a paradigm shift in organic semiconductor-based technologies[108] (reproduced with permission, copyright 2021, Springer Nature).

Although Fig. 14 does not depict the exact case of donor–acceptor polymers, it illustrates that these systems can be constructed from many different donor and acceptor moieties. This compositional flexibility allows broad tuning of key properties such as energy levels, charge–carrier mobility, and thermal conductivity. Understanding these structure–property relationships can be greatly facilitated by machine–learning models. Mapping the electronic structure to diverse molecular and physical descriptors will enable data–driven discovery of novel donor–acceptor combinations, offering a pathway to accelerate the development of high–performance organic semiconductors and potentially driving a paradigm shift in their technological applications. When constructing the database, it is important to first apply standard data cleaning procedures to ensure consistency, followed by classification of similar donors or acceptors (*e.g.*, DPP-type, PDI-type). Within these respective frameworks, regression, neural networks, or other predictive modeling can then be performed to more reliably analyze and predict polymer structures and properties. By integrating ML with high-throughput experiments and computational simulations, the development of next-generation donor–acceptor thermoelectric polymers can be significantly expedited, leading to cost-effective and high-performance solutions for energy conversion.

8. Summary

Favorable energy states created by the donor–acceptor sequence led to high carrier mobility in donor–acceptor polymers, and they have been extensively explored for photovoltaic energy conversion. Due to the same reason, donor–acceptor

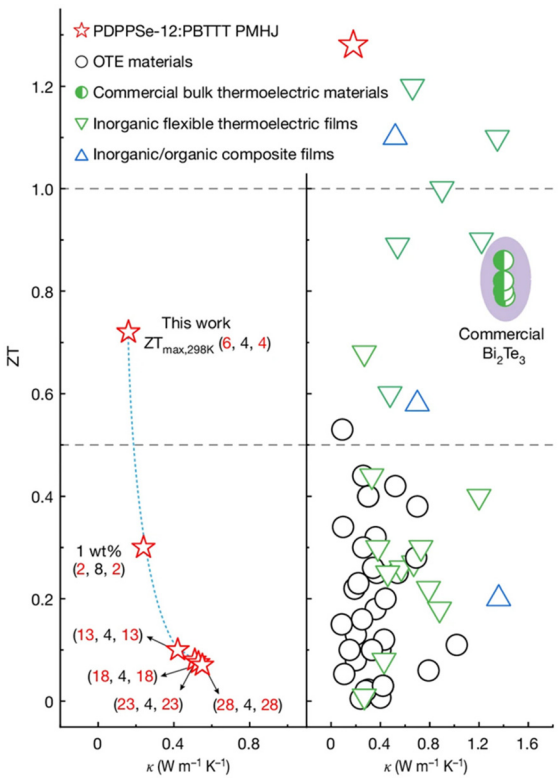

Fig. 15 Donor–acceptor polymer-based thermoelectric materials have demonstrated the highest performance among organic thermoelectrics, even approaching that of commercial thermoelectric materials (reproduced with permission, copyright 2025, Springer Nature).[109]

polymers are also attractive for thermoelectrics since a high σ can be achieved with a minimum amount of doping, which is important to maintain a high S as doping reduces S. While PEDOT:PSS has been widely explored as a p-type semiconductor, its n-type counterpart with similar performance has not been developed. Donor–acceptor polymers offer the advantage of being doped both p-type and n-type and, hence, are ideal for thermoelectrics. There is still a huge gap between the performance of organic and inorganic thermoelectrics. However, this gap is beginning to close. A recent breakthrough reported a record-high thermoelectric figure of merit (zT) of 0.6 at 298 K and 1.3 at 328 K for a donor–acceptor multi-heterojunction polymer fabricated *via* a periodic nanolayered architecture (Fig. 15).[109] This structure, which combines high charge mobility, suppressed in-plane k, and enhanced electronic entropy at the donor–acceptor interface, outperforms even commercial inorganic thermoelectrics near room temperature. To the best of our knowledge, this is highest performance ever reported in organic thermoelectric materials. Hence, donor–acceptor polymers have the potential to bridge the gap between organic and inorganic thermoelectrics while retaining all the attributes of organics such as flexibility and ease of manufacturing.

With proper measures, such as maintaining an open-shell and planar backbone with sidechains that favor inter-chain coupling, monomers that favor sharper DOS, and monomer sequences that favor a high S while maintaining high σ, a path forward can be adopted to achieve this milestone. To mechanistically explain thermoelectric property enhancement through mobility increase, the development of methods other than traditional Hall effect measurements is essential for accurate and independent determination of carrier concentration and mobility. Also, for proper evaluation of zT, accurate measurement of in-plane k is needed. Finally, developing a database on different synthesis conditions, structures, and properties of these polymers can enable the training of machine learning models that can facilitate the fabrication of these polymers with optimum thermoelectric properties. Thus, the integration of donor–acceptor polymers through precise molecular design, innovative characterization techniques, and data-driven optimization has the potential to revolutionize not only thermoelectrics but the entire field of organic semiconductors, paving the way for groundbreaking advancements in energy conversion, electronics, and beyond.

Conflicts of interest

There are no conflicts to declare.

Data availability

No primary research results, software or code have been included and no new data were generated or analysed as part of this review.

Acknowledgements

The authors gratefully acknowledged the support from DOE (Grant No. DE-EE0009771).

References

1 A. C. Gladen, X. Xiao, A. Zeller and Y. Yu, *J. Sol. Energy Eng.*, 2024, **146**, 051012.
2 Z. Bu, X. Zhang, Y. Hu, Z. Chen, S. Lin, W. Li, C. Xiao and Y. Pei, *Nat. Commun.*, 2022, **13**, 237.
3 Y. Jiang, J. Dong, H.-L. Zhuang, J. Yu, B. Su, H. Li, J. Pei, F.-H. Sun, M. Zhou, H. Hu, J.-W. Li, Z. Han, B.-P. Zhang, T. Mori and J.-F. Li, *Nat. Commun.*, 2022, **13**, 6087.
4 L. Shi, S. Chang and Z. Tian, *ACS Appl. Energy Mater.*, 2025, **8**, 25–30.
5 S. Chang, P. Biswas, Z. Qin and Z. Tian, *Small Methods*, 2024, **8**, 2400585.
6 J. Jing, L. Chopplet, N. Battaglini, V. Noël, B. Piro, T. Leydecker, Z. Wang, G. Mattana and E. Orgiu, *J. Mater. Chem. C*, 2024, **12**, 6185–6192.
7 X. He, C. Wu, T. Zhang, Z. Chen, L. Wang and J. Ouyang, *Adv. Funct. Mater.*, 2025, 2506872.
8 D. Yuan, W. Liu and X. Zhu, *Chem. Soc. Rev.*, 2023, **52**, 3842–3872.
9 C.-Y. Yang, M.-A. Stoeckel, T.-P. Ruoko, H.-Y. Wu, X. Liu, N. B. Kolhe, Z. Wu, Y. Puttisong, C. Musumeci, M. Massetti, H. Sun, K. Xu, D. Tu, W. M. Chen, H. Y. Woo, M. Fahlman, S. A. Jenekhe, M. Berggren and S. Fabiano, *Nat. Commun.*, 2021, **12**, 2354.
10 K. Broch, D. Venkateshvaran, V. Lemaur, Y. Olivier, D. Beljonne, M. Zelazny, I. Nasrallah, D. J. Harkin, M. Statz, R. D. Pietro, A. J. Kronemeijer and H. Sirringhaus, *Adv. Electron. Mater.*, 2017, **3**, 1700225.
11 A. Babel, Y. Zhu, K.-F. Cheng, W.-C. Chen and S. A. Jenekhe, *Adv. Funct. Mater.*, 2007, **17**, 2542–2549.
12 Y. Qin, C. Cheng, H. Geng, C. Wang, W. Hu, W. Xu, Z. Shuai and D. Zhu, *Phys. Chem. Chem. Phys.*, 2016, **18**, 14094–14103.
13 M. Ahn, M.-J. Kim, D. W. Cho and K.-R. Wee, *J. Org. Chem.*, 2021, **86**, 403–413.
14 Y. Zheng, R. Venkatesh, C. P. Callaway, C. Viersen, K. H. Fagbohungbe, A. L. Liu, C. Risko, E. Reichmanis and C. Silva-Acuña, *Chem. Mater.*, 2023, **35**, 10258–10267.
15 S. H. Kim, S. Park, S. Chung, E. Ok, B. J. Kim, J. D. Jang, B. Kang and K. Cho, *ACS Nano*, 2024, **18**, 31332–31348.
16 Y.-R. Shi and Y.-F. Liu, *Phys. Chem. Chem. Phys.*, 2019, **21**, 13304–13318.
17 J. O. Sofo and G. D. Mahan, *Phys. Rev. B:Condens. Matter Mater. Phys.*, 1994, **49**, 4565–4570.
18 S. Y. Son, J.-H. Kim, E. Song, K. Choi, J. Lee, K. Cho, T.-S. Kim and T. Park, *Macromolecules*, 2018, **51**, 2572–2579.
19 B. Carsten, J. M. Szarko, H. J. Son, W. Wang, L. Lu, F. He, B. S. Rolczynski, S. J. Lou, L. X. Chen and L. Yu, *J. Am. Chem. Soc.*, 2011, **133**, 20468–20475.

20 D. Beljonne, G. Pourtois, C. Silva, E. Hennebicq, L. M. Herz, R. H. Friend, G. D. Scholes, S. Setayesh, K. Müllen and J. L. Brédas, *Proc. Natl. Acad. Sci. U. S. A.*, 2002, **99**, 10982–10987.
21 H. Li, J. Song, J. Xiao, L. Wu, H. E. Katz and L. Chen, *Adv. Funct. Mater.*, 2020, **30**, 2004378.
22 C. Yang, W. Jin, J. Wang, Y. Ding, S. Nong, K. Shi, Y. Lu, Y. Dai, F. Zhuang, T. Lei, C. Di, D. Zhu, J. Wang and J. Pei, *Adv. Mater.*, 2018, **30**, 1802850.
23 H. Liu, Z. Liu, W. Jiang and H. Fu, *J. Solid State Chem.*, 2019, **274**, 47–51.
24 G. E. Gunbas, P. Camurlu, İ. M. Akhmedov, C. Tanyeli, A. M. Önal and L. Toppare, *J. Electroanal. Chem.*, 2008, **615**, 75–83.
25 J. Liu, L. Qiu, R. Alessandri, X. Qiu, G. Portale, J. Dong, W. Talsma, G. Ye, A. A. Sengrian, P. C. T. Souza, M. A. Loi, R. C. Chiechi, S. J. Marrink, J. C. Hummelen and L. J. A. Koster, *Adv. Mater.*, 2018, **30**, 1704630.
26 Y. Lu, Z.-D. Yu, Y. Liu, Y.-F. Ding, C.-Y. Yang, Z.-F. Yao, Z.-Y. Wang, H.-Y. You, X.-F. Cheng, B. Tang, J.-Y. Wang and J. Pei, *J. Am. Chem. Soc.*, 2020, **142**, 15340–15348.
27 C. Francis, D. Fazzi, S. B. Grimm, F. Paulus, S. Beck, S. Hillebrandt, A. Pucci and J. Zaumseil, *J. Mater. Chem. C*, 2017, **5**, 6176–6184.
28 W. Shi, T. Deng, Z. M. Wong, G. Wu and S.-W. Yang, *npj Comput. Mater.*, 2021, **7**, 1–8.
29 E. H. Hasdeo, L. P. A. Krisna, M. Y. Hanna, B. E. Gunara, N. T. Hung and A. R. T. Nugraha, *J. Appl. Phys.*, 2019, **126**, 035109.
30 J. Park, Y. Xia, V. Ozoliņš and A. Jain, *npj Comput. Mater.*, 2021, **7**, 1–9.
31 X. Yong, G. Wu, W. Shi, Z. M. Wong, T. Deng, Q. Zhu, X. Yang, J.-S. Wang, J. Xu and S.-W. Yang, *J. Mater. Chem. A*, 2020, **8**, 21852–21861.
32 Z. Tian, S. Lee and G. Chen, *J. Heat Transfer*, 2013, **135**, 061605.
33 J. P. Heremans, V. Jovovic, E. S. Toberer, A. Saramat, K. Kurosaki, A. Charoenphakdee, S. Yamanaka and G. J. Snyder, *Science*, 2008, **321**, 554–557.
34 J. Liu, G. Ye, B. van der Zee, J. Dong, X. Qiu, Y. Liu, G. Portale, R. C. Chiechi and L. J. A. Koster, *Adv. Mater.*, 2018, **30**, 1804290.
35 J. Wu, S. Yang, S. Wang, Z. Jiang, C. Gao and L. Wang, *Compos. Commun.*, 2023, **37**, 101461.
36 L. Tu, J. Wang, Z. Wu, J. Li, W. Yang, B. Liu, S. Wu, X. Xia, Y. Wang, H. Y. Woo and Y. Shi, *Angew. Chem.*, 2024, **136**, e202319658.
37 H. J. Cheon, T. S. Lee, J. E. Lee, S. B. Kim, E. H. Suh, S.-K. Kwon, Y. J. Jeong, J. Jang and Y.-H. Kim, *Chem. Mater.*, 2023, **35**, 1796–1805.
38 B. Yu, M. Zebarjadi, H. Wang, K. Lukas, H. Wang, D. Wang, C. Opeil, M. Dresselhaus, G. Chen and Z. Ren, *Nano Lett.*, 2012, **12**, 2077–2082.
39 K. S. Mayer, D. J. Adams, N. Eedugurala, M. M. Lockart, P. Mahalingavelar, L. Huang, L. A. Galuska, E. R. King, X. Gu, M. K. Bowman and J. D. Azoulay, *Cell Rep. Phys. Sci.*, 2021, **2**, 100467.
40 A. E. London, H. Chen, M. A. Sabuj, J. Tropp, M. Saghayezhian, N. Eedugurala, B. A. Zhang, Y. Liu, X. Gu, B. M. Wong, N. Rai, M. K. Bowman and J. D. Azoulay, *Sci. Adv.*, 2019, **5**, eaav2336.
41 K. Yang, X. Zhang, A. Harbuzaru, L. Wang, Y. Wang, C. Koh, H. Guo, Y. Shi, J. Chen, H. Sun, K. Feng, M. C. Ruiz Delgado, H. Y. Woo, R. P. Ortiz and X. Guo, *J. Am. Chem. Soc.*, 2020, **142**, 4329–4340.
42 H. Tang, Z. Liu, Y. Tang, Z. Du, Y. Liang, Z. Hu, K. Zhang, F. Huang and Y. Cao, *Giant*, 2021, **6**, 100053.
43 L. Huang, N. Eedugurala, A. Benasco, S. Zhang, K. S. Mayer, D. J. Adams, B. Fowler, M. M. Lockart, M. Saghayezhian, H. Tahir, E. R. King, S. Morgan, M. K. Bowman, X. Gu and J. D. Azoulay, *Adv. Funct. Mater.*, 2020, **30**, 1909805.
44 X.-X. Chen, J.-T. Li, Y.-H. Fang, X.-Y. Deng, X.-Q. Wang, G. Liu, Y. Wang, X. Gu, S.-D. Jiang and T. Lei, *Nat. Commun.*, 2022, **13**, 2258.
45 Y. Joo, L. Huang, N. Eedugurala, A. E. London, A. Kumar, B. M. Wong, B. W. Boudouris and J. D. Azoulay, *Macromolecules*, 2018, **51**, 3886–3894.
46 R. Wu, Y. Wei, X. Dai, L. Yan, W. Liu, D. Yuan, J. Zhu and X. Zhu, *Angew. Chem., Int. Ed.*, 2025, **64**, e202413061.
47 J. Wu, X. Yin, F. Yang, S. Wang, Y. Liu, X. Mao, X. Nie, S. Yang, C. Gao and L. Wang, *Chem. Eng. J.*, 2022, **429**, 132354.
48 S. E. Yoon, S. J. Shin, S. Y. Lee, G. G. Jeon, H. Kang, H. Seo, J. Zheng and J. H. Kim, *ACS Appl. Polym. Mater.*, 2020, **2**, 2729–2735.
49 S. Kohno, Y. Yamashita, N. Kasuya, T. Mikie, I. Osaka, K. Takimiya, J. Takeya and S. Watanabe, *Commun. Mater.*, 2020, **1**, 1–8.
50 S. Chuo, Y.-C. Peng, T. Puangniyom, Q.-G. Chen, C.-C. Chueh and W.-Y. Lee, *RSC Appl. Interfaces*, 2024, **1**, 1012–1019.
51 F. Günther, S. Gemming and G. Seifert, *J. Phys. Chem. C*, 2016, **120**, 9581–9587.
52 J. M. Frost, F. Cheynis, S. M. Tuladhar and J. Nelson, *Nano Lett.*, 2006, **6**, 1674–1681.
53 Y. Liu, R. Chen, J. Li, X. Liu, H. Li and Y. Han, *ACS Appl. Mater. Interfaces*, 2025, **17**, 1711–1724.
54 C. Zhu, A. J. Kalin and L. Fang, *Acc. Chem. Res.*, 2019, **52**, 1089–1100.
55 S.-Y. Jang, I.-B. Kim, J. Kim, D. Khim, E. Jung, B. Kang, B. Lim, Y.-A. Kim, Y. H. Jang, K. Cho and D.-Y. Kim, *Chem. Mater.*, 2014, **26**, 6907–6910.
56 M. Pei, J.-H. Kim, S. On, H.-K. Lee, K. Cho, D.-H. Hwang and H. Yang, *Macromol. Chem. Phys.*, 2017, **218**, 1700135.
57 S. Wang, H. Sun, T. Erdmann, G. Wang, D. Fazzi, U. Lappan, Y. Puttisong, Z. Chen, M. Berggren, X. Crispin, A. Kiriy, B. Voit, T. J. Marks, S. Fabiano and A. Facchetti, *Adv. Mater.*, 2018, **30**, 1801898.
58 Y.-J. Kim, N.-K. Kim, W.-T. Park, C. Liu, Y.-Y. Noh and D.-Y. Kim, *Adv. Funct. Mater.*, 2019, **29**, 1807786.

59 J. Y. Oh, M. Shin, T. I. Lee, W. S. Jang, Y. Min, J.-M. Myoung, H. K. Baik and U. Jeong, *Macromolecules*, 2012, **45**, 7504–7513.
60 J. Hynynen, E. Järsvall, R. Kroon, Y. Zhang, S. Barlow, S. R. Marder, M. Kemerink, A. Lund and C. Müller, *ACS Macro Lett.*, 2019, **8**, 70–76.
61 K. Tremel, F. S. U. Fischer, N. Kayunkid, R. D. Pietro, R. Tkachov, A. Kiriy, D. Neher, S. Ludwigs and M. Brinkmann, *Adv. Energy Mater.*, 2014, **4**, 1301659.
62 L. H. Jimison, M. F. Toney, I. McCulloch, M. Heeney and A. Salleo, *Adv. Mater.*, 2009, **21**, 1568–1572.
63 A. Salleo, R. J. Kline, D. M. DeLongchamp and M. L. Chabinyc, *Adv. Mater.*, 2010, **22**, 3812–3838.
64 R. J. Kline and M. D. McGehee, *Polym. Rev.*, 2006, **46**, 27–45.
65 H. M. Schrickx, P. Sen, N. Balar and B. T. O'Connor, *CR-PHYS-SC*, 2024, **5**, 102076.
66 L. Biniek, S. Pouget, D. Djurado, E. Gonthier, K. Tremel, N. Kayunkid, E. Zaborova, N. Crespo-Monteiro, O. Boyron, N. Leclerc, S. Ludwigs and M. Brinkmann, *Macromolecules*, 2014, **47**, 3871–3879.
67 D. Kim, S. B. Lee, M.-J. Kim, J. Lee, S. Chung, E. Ok, G. Lee, J. Min, K. Cho and B. Kang, *Small Methods*, 2023, **7**, 2300256.
68 G. Ren, Z. Wang, X. Huang, D. Hur, M. A. Pfeifer, M. N. Silberstein and Z. Tian, *Mater. Horiz.*, 2025, **12**, 2957–2964.
69 Y. Lu, J.-Y. Wang and J. Pei, *Chem. Mater.*, 2019, **31**, 6412–6423.
70 T. S. Lee, S. B. Lee, D.-Y. Choi, E. H. Suh, T. K. An, Y. J. Jeong, J. Jang and Y.-H. Kim, *Macromol. Res.*, 2021, **29**, 887–894.
71 M. L. Tietze, J. Benduhn, P. Pahner, B. Nell, M. Schwarze, H. Kleemann, M. Krammer, K. Zojer, K. Vandewal and K. Leo, *Nat. Commun.*, 2018, **9**, 1182.
72 W. Zhao, J. Ding, Y. Zou, C. Di and D. Zhu, *Chem. Soc. Rev.*, 2020, **49**, 7210–7228.
73 Y. Zeng, W. Zheng, Y. Guo, G. Han and Y. Yi, *J. Mater. Chem. A*, 2020, **8**, 8323–8328.
74 H. Guo, C.-Y. Yang, X. Zhang, A. Motta, K. Feng, Y. Xia, Y. Shi, Z. Wu, K. Yang, J. Chen, Q. Liao, Y. Tang, H. Sun, H. Y. Woo, S. Fabiano, A. Facchetti and X. Guo, *Nature*, 2021, **599**, 67–73.
75 X.-Y. Wang, Y.-F. Ding, X.-Y. Zhang, Y.-Y. Zhou, C.-K. Pan, Y.-H. Li, N.-F. Liu, Z.-F. Yao, Y.-S. Chen, Z.-H. Xie, Y.-F. Huang, Y.-C. Xu, H.-T. Wu, C.-X. Huang, M. Xiong, L. Ding, Z.-D. Yu, Q.-Y. Li, Y.-Q. Zheng, J.-Y. Wang and J. Pei, *Nature*, 2025, **642**, 599–604.
76 C.-Y. Yang, Y.-F. Ding, D. Huang, J. Wang, Z.-F. Yao, C.-X. Huang, Y. Lu, H.-I. Un, F.-D. Zhuang, J.-H. Dou, C. Di, D. Zhu, J.-Y. Wang, T. Lei and J. Pei, *Nat. Commun.*, 2020, **11**, 3292.
77 J. A. Ávila-Niño, E. Araujo and F. González, *Synth. Met.*, 2023, **299**, 117465.
78 M. A. Leaf and M. Muthukumar, *Macromolecules*, 2016, **49**, 4286–4294.
79 D. Ju, D. Kim, H. Yook, J. W. Han and K. Cho, *Adv. Funct. Mater.*, 2019, **29**, 1905590.
80 J. Yamamoto and Y. Furukawa, *J. Phys. Chem. B*, 2015, **119**, 4788–4794.
81 Y. Zhong, V. Untilova, D. Muller, S. Guchait, C. Kiefer, L. Herrmann, N. Zimmermann, M. Brosset, T. Heiser and M. Brinkmann, *Adv. Funct. Mater.*, 2022, **32**, 2202075.
82 S. B. Kim, S. Song, T. S. Lee, M. K. A. Joenata, E. H. Suh, Y. J. Jeong, J. Jang and Y.-H. Kim, *J. Mater. Chem. C*, 2024, **12**, 9227–9235.
83 J.-F. Ding, K. Yamanaka, S.-H. Hong, G.-L. Chen, W.-N. Wu, J.-M. Lin, S.-H. Tung, I. Osaka and C.-L. Liu, *Adv. Sci.*, 2024, **11**, 2410046.
84 C.-H. Tsai, Y.-C. Lin, W.-N. Wu, S.-H. Tung, W.-C. Chen and C.-L. Liu, *J. Mater. Chem. C*, 2023, **11**, 6874–6883.
85 H. Zhou, C. Gao, T. Liu, C. Pan and L. Wang, *J. Mater. Chem. C*, 2020, **8**, 7096–7103.
86 I. H. Jung, C. T. Hong, U.-H. Lee, Y. H. Kang, K.-S. Jang and S. Y. Cho, *Sci. Rep.*, 2017, **7**, 44704.
87 T. Kolodiazhnyi, A. Petric, M. Niewczas, C. Bridges, A. Safa-Sefat and J. E. Greedan, *Phys. Rev. B:Condens. Matter Mater. Phys.*, 2003, **68**, 085205.
88 G. J. Snyder, A. H. Snyder, M. Wood, R. Gurunathan, B. H. Snyder and C. Niu, *Adv. Mater.*, 2020, **32**, 2001537.
89 Y. Xiao, L. Xu, T. Hong, H. Shi, S. Wang, X. Gao, X. Ding, J. Sun and L.-D. Zhao, *Energy Environ. Sci.*, 2022, **15**, 346–355.
90 M. Alejandra Hermosilla-Palacios, M. Martinez, E. A. Doud, T. Hertel, A. M. Spokoyny, S. Cambré, W. Wenseleers, Y.-H. Kim, A. J. Ferguson and J. L. Blackburn, *Nanoscale Horiz.*, 2024, **9**, 278–284.
91 H. Bässler, D. Kroh, F. Schauer, V. Nádaždy and A. Köhler, *Adv. Funct. Mater.*, 2021, **31**, 2007738.
92 C. Huang, X. Qian and R. Yang, *Mater. Sci. Eng., R*, 2018, **132**, 1–22.
93 R. J. Warzoha, A. A. Wilson, B. F. Donovan, N. Donmezer, A. Giri, P. E. Hopkins, S. Choi, D. Pahinkar, J. Shi, S. Graham, Z. Tian and L. Ruppalt, *J. Electron. Packag.*, 2021, **143**, 020804.
94 H. Ma and Z. Tian, *Appl. Phys. Lett.*, 2015, **107**, 073111.
95 H. Ma, Y. Ma and Z. Tian, *ACS Appl. Polym. Mater.*, 2019, **1**, 2566–2570.
96 J. Liu, X. Wang, D. Li, N. E. Coates, R. A. Segalman and D. G. Cahill, *Macromolecules*, 2015, **48**, 585–591.
97 H. Ma and Z. Tian, *Appl. Phys. Lett.*, 2017, **110**, 091903.
98 X. Wei, Z. Wang, Z. Tian and T. Luo, *J. Heat Transfer*, 2021, **143**, 072101.
99 H. Ma, E. O'Donnel and Z. Tian, *Nanoscale*, 2018, **10**, 13924–13929.
100 Q. Wei, M. Mukaida, K. Kirihara and T. Ishida, *ACS Macro Lett.*, 2014, **3**, 948–952.
101 C. Li, H. Ma and Z. Tian, *Appl. Therm. Eng.*, 2017, **111**, 1441–1447.
102 Q. Fang, K. Yi, T. Zhai, S. Luo, C. Lin, Q. Ai, Y. Zhu, B. Zhang, G. A. Alvarez, Y. Shao, H. Zhou, G. Gao, Y. Liu, R. Xu, X. Zhang, Y. Wang, X. Tian, H. Zhang, Y. Han,

H. Zhu, Y. Zhao, Z. Tian, Y. Zhong, Z. Liu and J. Lou, *Nat. Commun.*, 2024, **15**, 10780.
103 J. J. Urban, A. K. Menon, Z. Tian, A. Jain and K. Hippalgaonkar, *J. Appl. Phys.*, 2019, **125**, 180902.
104 K. Kranthiraja and A. Saeki, *ACS Appl. Mater. Interfaces*, 2022, **14**, 28936–28944.
105 R. Machaka, G. T. Motsi, L. M. Raganya, P. M. Radingoana and S. Chikosha, *Data Brief*, 2021, **38**, 107346.
106 Q. Tao, P. Xu, M. Li and W. Lu, *npj Comput. Mater.*, 2021, **7**, 1–18.
107 J. S. De Vos, S. Ravichandran, S. Borgmans, L. Vanduyfhuys, P. Van Der Voort, S. M. J. Rogge and V. Van Speybroeck, *Chem. Mater.*, 2024, **36**, 4315–4330.
108 C. Kunkel, J. T. Margraf, K. Chen, H. Oberhofer and K. Reuter, *Nat. Commun.*, 2021, **12**, 2422.
109 D. Wang, J. Ding, Y. Ma, C. Xu, Z. Li, X. Zhang, Y. Zhao, Y. Zhao, Y. Di, L. Liu, X. Dai, Y. Zou, B. Kim, F. Zhang, Z. Liu, I. McCulloch, M. Lee, C. Chang, X. Yang, D. Wang, D. Zhang, L.-D. Zhao, C. Di and D. Zhu, *Nature*, 2024, **632**, 528–535.